Molecular-dynamics study of phase transitions in alkali azides

M. M. Ossowski and J. R. Hardy
Department of Physics and Center for Electro-Optics, University of Nebraska, Lincoln, Nebraska 68588-0111

R. W. Smith
Department of Chemistry, University of Nebraska, Omaha, Nebraska 68182-0109

(Received 18 June 1999)

An account is presented of our studies of the order-disorder phase transitions in KN_3, RbN_3, and CsN_3. These are based on parameter-free interionic potentials based on the Gordon-Kim modified electron-gas formalism extended to molecular ions. We performed static structural relaxations and supercell molecular dynamics and predicted with reasonable accuracy the temperatures for the onset of the transitions. In particular, we address the question of how the N_3^- ions reorient to yield the transitions. We found the existence of NaCl-type high-temperature phases in disordered KN_3 and RbN_3 and argue that this restructuring is preempted by melting in these two systems. [S0163-1829(99)10541-1]

I. INTRODUCTION

Alkali azides, salts with linear N_3^- anions, have been extensively studied in recent years.[1] The majority of alkali azides exhibit simple spatial symmetry, but since they have an internal molecular structure, they are logical candidates to study, following alkali halides and cyanides (CN^-). Of special interest, from the theoretical point of view, is the order-disorder phase transition observed in most of these systems before melting. In particular, there exists a substantial disagreement on the microscopic mechanism of these transitions.[1] In order to address this question we present results of a molecular-dynamics (MD) study performed on three isostructural azides, KN_3, RbN_3, and CsN_3. In particular, we investigate how the dynamics of the N_3^- molecular ions drives the phase transformations in these materials.

In prior work,[2] we have developed a first-principles model, based on the Gordon-Kim (GK) modified electron-gas formalism,[3] for the interionic and intraionic potentials within ionic molecular crystals. The details of this approach are described elsewhere.[2] In this paper we only outline the method to highlight points specific to the systems under consideration.

The method starts from the quantum chemistry optimization performed for the whole molecular ion N_3^-, using the GAUSSIAN94 (Ref. 4) commercial package and Hartree-Fock algorithm with the standard 6-31G* basis for center and end nitrogens. The resulting molecular charge density is then decomposed onto the nitrogen centers of the N_3^- ion in the spirit of a Mulliken population analysis.[5] This determination of the nitrogen ion monopole charges combined with the spherical averaging of the charge distributions enables us to compute the interionic GK pair-potentials. For charge density of alkali ions we used the Clementi tables.[6]

The intraionic forces are treated within the harmonic approximation whose coefficient are determined by the GAUSSIAN94 package while the long-range Coulomb interactions are computed from the fractional ionicities for the center and end nitrogens: $+0.3022$ and -0.6511, respectively, and $+1$ for alkali cations.

II. ROOM-TEMPERATURE PHASES AND THE ORDER-DISORDER PHASE TRANSITIONS IN KN_3, RbN_3, AND CsN_3

The room-temperature phase of KN_3, RbN_3, and CsN_3 has a body-centered tetragonal structure of space group $I4/mcm(Z=4)$ in which the azide ions are perfectly ordered along two distinctive crystallographic directions.[7,8] This phase is, in fact, the CsCl $Pm\bar{3}m$ structure tetragonally distorted to allow for the asphericity of the N_3^- ions. As the temperature is raised, at ambient pressure, RbN_3 and CsN_3 transform at 588 and 424 K, respectively, into a disordered phase and melt at 590 and 599 K.[9] No such transformation has been observed in KN_3. The nature and extent of the N_3^- disordering as well as the determination of the high-temperature modification of RbN_3 still remains speculative, whereas the high-temperature phase of CsN_3 has been reported from x-ray powder diffraction as having $Pm\bar{3}m$ symmetry.[9] In this phase the linear azide ions are inferred to be oriented at random with respect to the edges of the cubic unit cell.[9] This presumption was more recently supported by Raman-scattering studies in RbN_3 and CsN_3.[10,11]

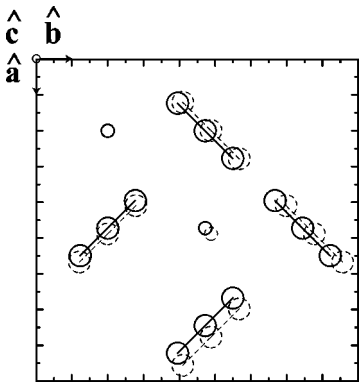

FIG. 1. Projection along c of the theoretical structure of KN_3 in the $I4/mcm$ phase. Broken lines depict the same structure determined experimentally.

TABLE I. Prototypic atomic positions in the relaxed structures of KN_3, RbN_3, and CsN_3. Experimental values (Ref. 7) are given in parentheses.

Prototype	x/a	y/b	z/c	Wyckoff
N(2) in KN_3	0.1414(0.1365)	0.5+0.1414(0.1365)	0	8(h)
N(2) in RbN_3	0.1376(0.1310)	0.5+0.1376(0.1310)	0	8(h)
N(2) in CsN_3	0.1334(0.1260)	0.5+0.1334(0.1260)	0	8(h)

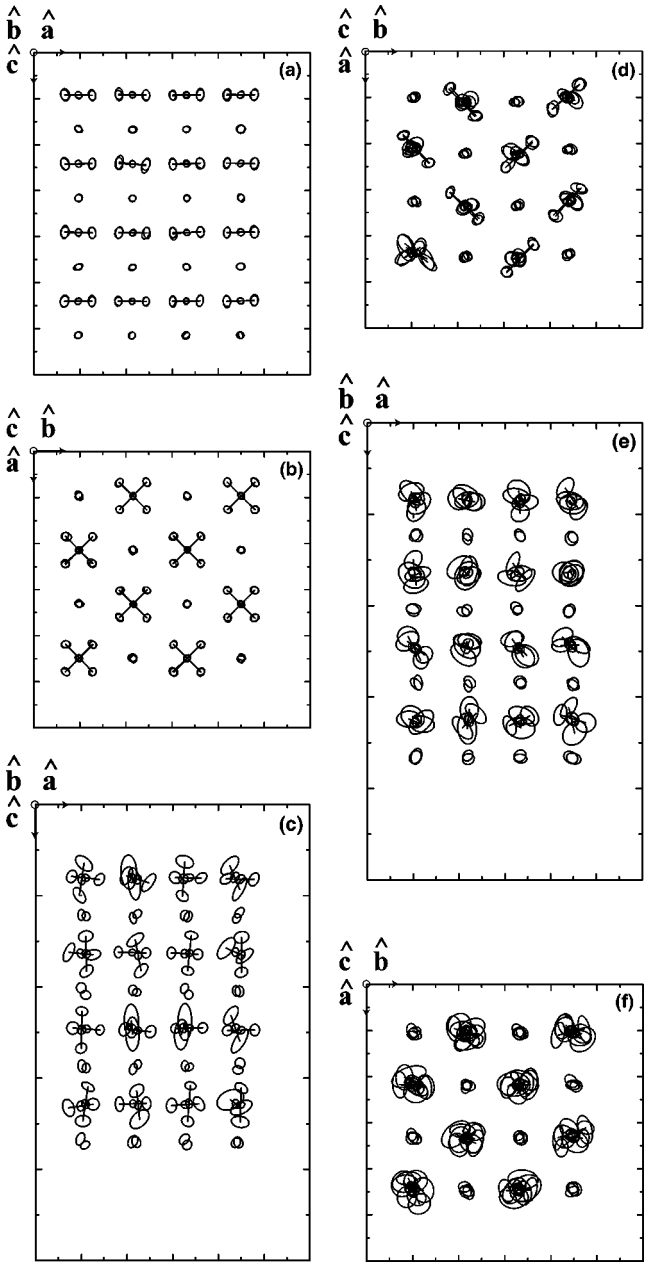

FIG. 2. Projections of the atomic positions along the tetragonal b and c axes in the average structure of CsN_3 obtained from the MD simulation discussed in the text. The ''thermal ellipsoids'' indicate the rms deviation of atoms from their average positions and represent the thermal motions of the atoms. Bonds connect the average positions of the center nitrogen atoms with the end nitrogen atoms in the N_3^- ion. (a,b) 484 K, (c,d) 464 K, and (e,f) 477 K.

III. STATIC RELAXATION OF THE ROOM-TEMPERATURE *I*4/*mcm* PHASES

Using the intraionic and interionic pair potentials obtained as described in Sec. I, we first performed static relaxations for the room-temperature phases of KN_3, RbN_3, and CsN_3. This procedure determines the positions of atoms and the lattice vectors that correspond to the minimum of the theoretical potential-energy surface, employing a Newton-Raphson–type algorithm. It is performed for an infinite lattice by applying periodic boundary conditions. The standard Ewald technique is used to handle the Coulomb forces.

Supercells, like the KN_3 supercell shown in Fig. 1, which are equivalent to the crystallographic unit cells for the room-temperature phases of KN_3, RbN_3, and CsN_3 were used in the minimizations. Table I lists prototype atomic positions as well as the lattice constants obtained by relaxation with the *I*4/*mcm* symmetry constraints for the three azides and compares them with experiment. Agreement between the lattice constants is within 5% for all the azides. An average 5% shortening of the lattice has been a rather general feature observed in our other work with GK potentials.[2] Also, the experimental values of these parameters are room-temperature values and thus include the effects of thermal expansion. For example, as will be shown in the next section, in a molecular-dynamics run on KN_3, a and c increase by 0.7% and 2.1%, respectively, between 0–300 K.

The discrepancies in fractional atomic positions are well within the thermal fluctuations of the atoms at room temperature and amount to 2%, 1%, and 1% shortening of the N-N bond lengths in KN_3, RbN_3, and CsN_3, respectively.

We also performed static relaxations without the *I*4/*mcm*

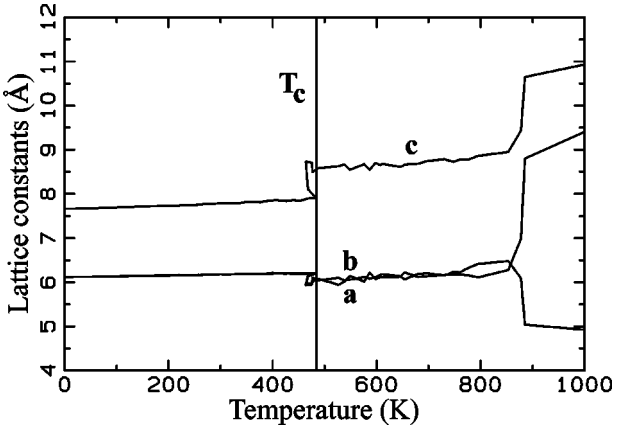

FIG. 3. Lattice constants as a function of temperature for the MD run on CsN_3. Notice that $c'=c\cong\sqrt{2}a=a'=b'$ above T_c, which indicates the average CsCl phase for the disordered CsN_3.

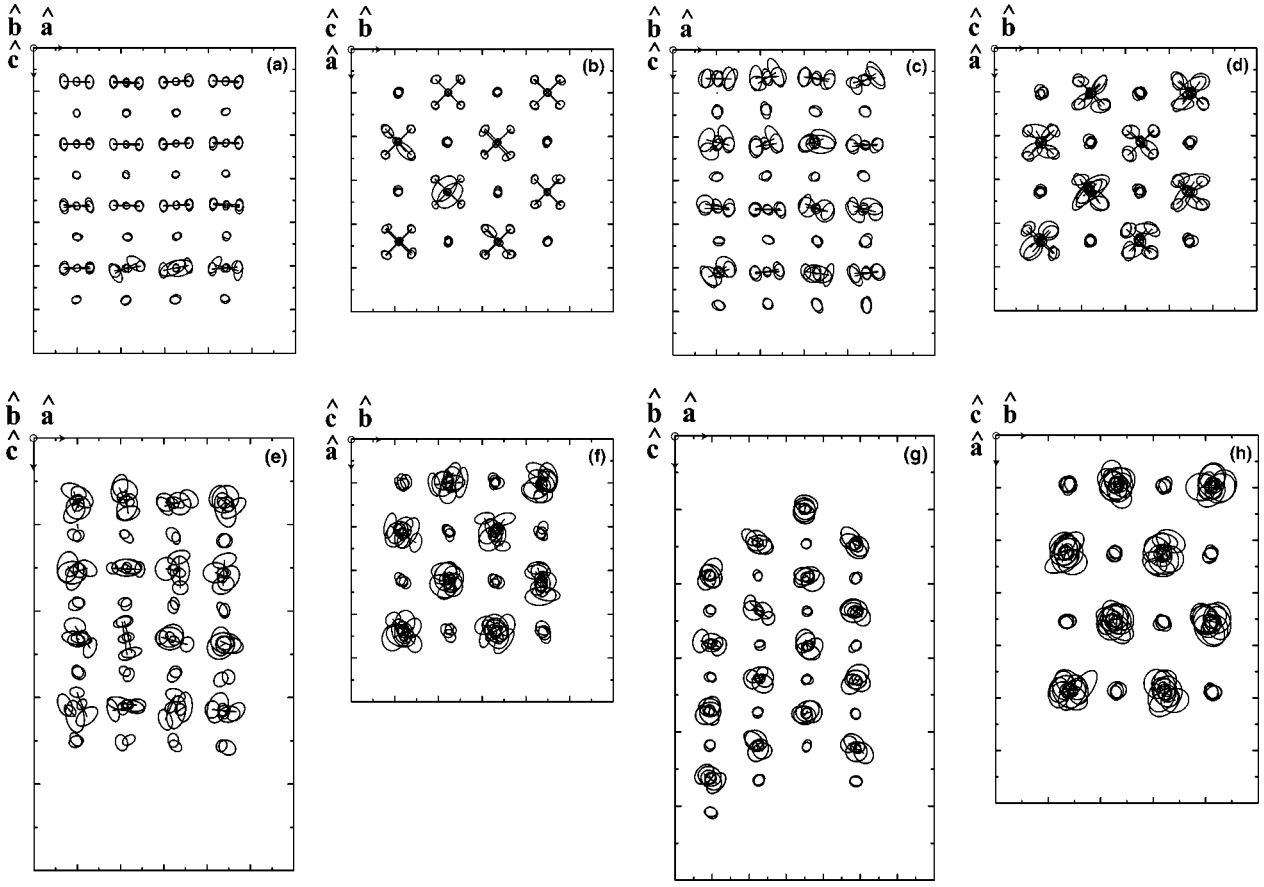

FIG. 4. Projections of the atomic positions along the tetragonal *b* and *c* axes in the average structure of RbN_3 obtained from the MD simulation discussed in the text. (a,b) 618 K, (c,d) 613 K, (e,f) 603 K, (g,h) 664 K.

symmetry constraints, and in all cases exactly reproduced the relaxed structures obtained with the symmetry constraints.

IV. MOLECULAR-DYNAMICS SIMULATIONS OF THE PHASE TRANSITIONS (REF. 12)

These potentials were then employed in molecular-dynamics simulations. These runs were initiated on 128 atoms supercells obtained from doubling the statically relaxed room-temperature symmetry cells of the three azides in all three directions. Our constant-energy MD follows the Verlet algorithm with periodic boundary conditions and Ewald summation for lattice energy and forces. As the first step we removed any residual energy by ''quenching'' the supercell to 0 K thus ensuring that a MD run starts from the ground state of the system. Following this ''quench,'' the system was ''heated'' by injecting kinetic energy in steps equivalent to ~5 K. After each ''pulse'' the supercell was left to equilibrate for 12 ps. The molecular-dynamics time step used was 0.001 ps and a typical run from 0 to ~1000 K on one R10000 ® CPU running at 195 MHz took about two weeks.

We first looked at CsN_3 as this azide has a well-established high-temperature phase.[9] Figure 2 shows a series of cross sections along two orthogonal directions associated with the *b* and *c* axes of the *tetragonal* room-temperature unit cell. Figures 2(a) and 2(b) show an ordered system approaching T_c. Large ovals centered about the atoms represent ''thermal ellipsoids,'' which indicate rms deviation of atoms from their average positions. Although, on average, the N_3^- ions remain in the *ab* plane pointing in the two distinctive directions, as in the room-temperature tetragonal phase, we already notice a tendency among them to move into regions disallowed by the $I4/mcm$ symmetry, namely out of the *ab* plane. This tendency becomes more pronounced as the disordering proceeds and in Figs. 2(c) and 2(d) we see half of the N_3^- ions rotated 90° from the *ab* plane. These ions now progressively occupy space between

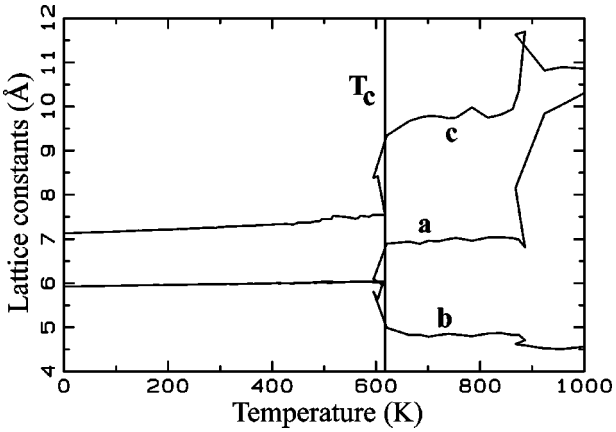

FIG. 5. Lattice constants as a function of temperature for the MD run on RbN_3. See Fig. 6 for the description of the structural transformation.

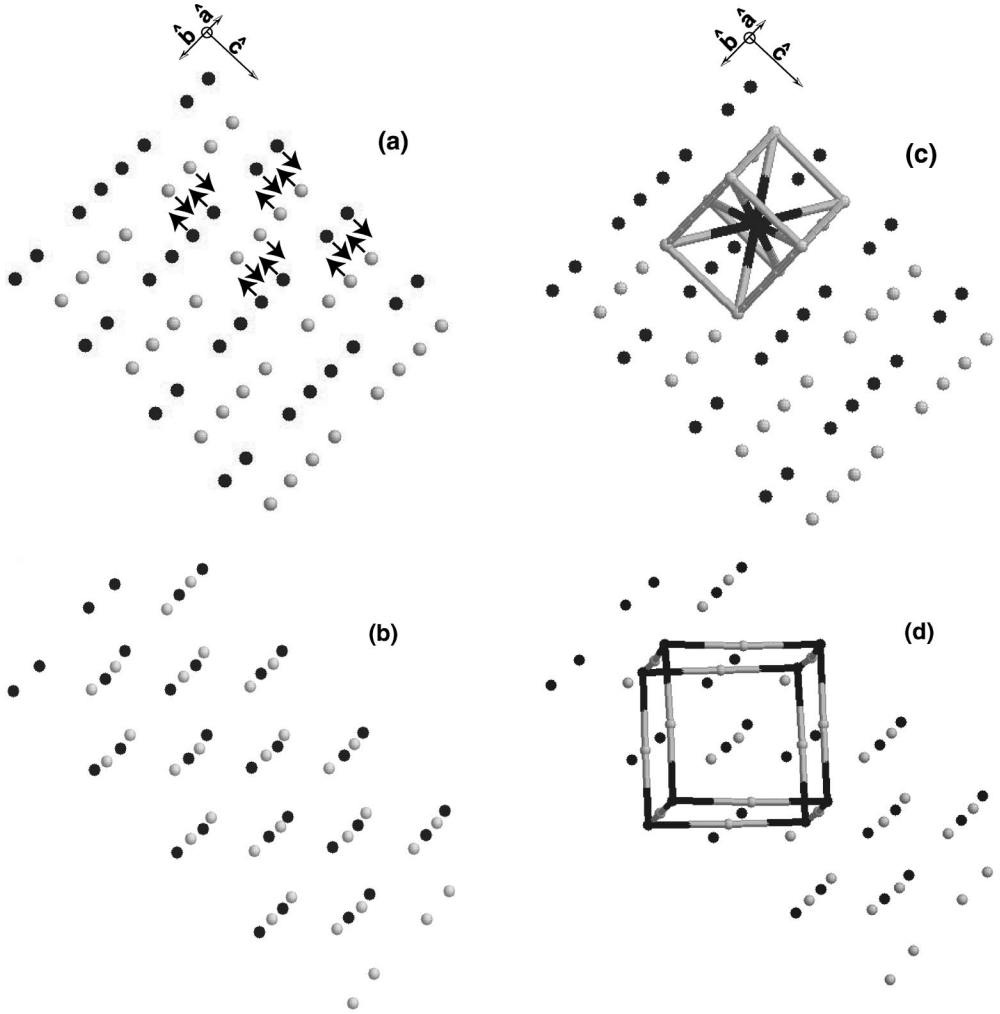

FIG. 6. Schematic of the reconstructing of the RbN_3 and KN_3 into the high-temperature average NaCl phase. Black circles denote the center nitrogen atoms of the N_3^- ions while the end nitrogen were stripped for clarity. The *tetragonal* lattice vectors are drawn only for the room-temperature $I4/mcm$ structure (a) and (c). In the high-temperature average $Fm\bar{3}m$ structure (d) the new lattice vectors may be assigned along the edges of the cube. The transformation occurs as layers of N_3^- ions and cations that lie in *bc* planes with distinctive coordinates along *a* direction slide on top of each other and destroy the original room-temperature layered arrangement along the *c* axis in which the N_3^- ions were sandwiched in between the cations (a). This produces, given the rotational disordering of the N_3^- ions, the average NaCl structure (b). The CsCl-like unit cell in the room-temperature phase is shown (c) as well as the average NaCl unit cell in the high-temperature phase (d).

the original N_3^- layers (of the room-temperature tetragonal phase). This causes the lattice to expand along the tetragonal *c* axis as illustrated in Fig. 3, which shows lattice constants as a function of temperature for the MD run on CsN_3, from $T=0$ K to ''melting'' at $\sim$1000 K. After the lattice has expanded sufficiently, the N_3^- ions can perform random hindered rotations about all three spatial axes, as shown in Figs. 2(e) and 2(f). The disordering is now complete and the system has transformed to a new high-temperature phase of the average CsCl symmetry following expansion along *c* and contraction along *a* and *b*.

A more complicated picture emerges for KN_3 and RbN_3. Figure 4 shows a set of cross sections, along the *b* and *c* axes of the room-temperature tetragonal phase, for the RbN_3 supercell. The cross sections in Fig. 4(a) and 4(b) show the supercell approaching the T_c. The N_3^- ions are on average still in the ordered state pointing in the two distinctive directions in the *ab* plane. However, in the next cross sections shown in Figs. 4(c) and 4(d), we see the N_3^- ions unlocking from their room-temperature positions through hindered rotations, mainly out of the *ab* plane. Next, as shown in Figs. 4(e) and 4(f), hindered rotations in the *ab* plane occur, in addition to those out of the *ab* plane. During this gradual disordering of the N_3^- ions the lattice expands, as seen in Fig. 5, but does so in a more dramatic way than in case of CsN_3. We find that the volume change of the supercell above T_c in RbN_3 is $\sim$19% in contrast to $\sim$4% in CsN_3. In addition to N_3^- disordering we have a restructuring from a tetragonal phase to an average NaCl phase, as shown in Figs. 4(g) and 4(h). This restructuring is illustrated in Figs. 6(a) and 6(b) while in Figs. 6(c) and 6(d) we show both room-temperature CsCl and high-temperature NaCl unit cells. The appearance of this new high-temperature phase is a novelty in the sense that a structural phase transition of this sort has not been observed experimentally to our knowledge.

A similar behavior was observed in our simulations for

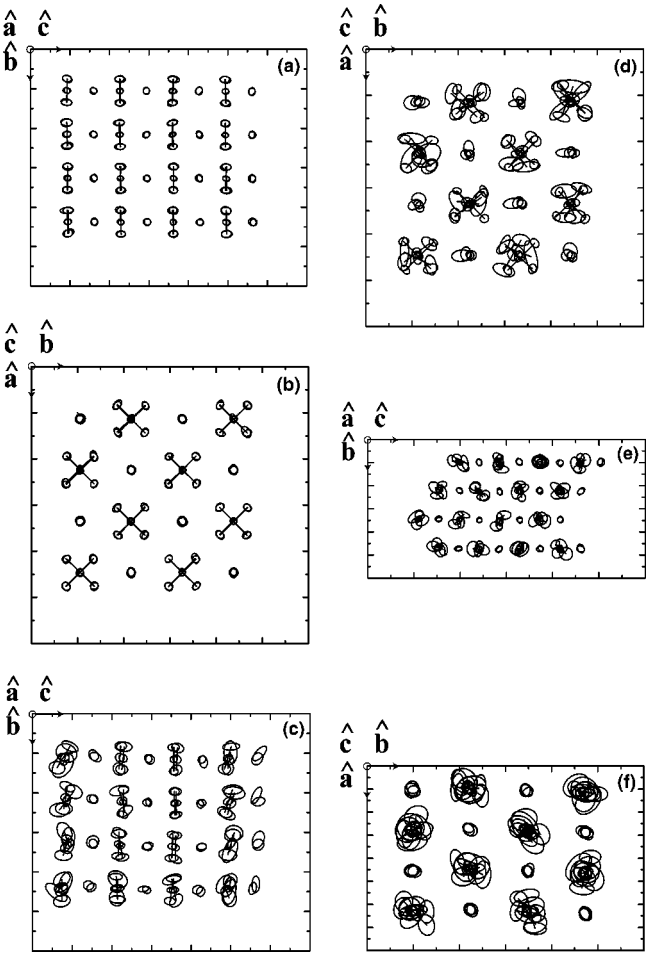

FIG. 7. Projections of the atomic positions along the tetragonal *a* and *c* axes in the average structures of CsN_3 obtained from the MD simulation discussed in the text. (a,b) 602 K, (c,d) 561 K, (e,f) 577 K.

KN_3. Figure 7 shows the cross sections, along the *a* and *c* axes of the room-temperature tetragonal phase, of the average atomic positions for the KN_3 supercell as the system undergoes the order-disorder transition. The difference for KN_3 compared with RbN_3 is that the transition seems to occur more suddenly with N_3^- disordering both in and out of the *ab* plane commencing simultaneously, as can be seen in Figs. 7(c) and 7(d). As in the case of RbN_3, the disordering of the N_3^- ions appears to force a structural transformation from the room-temperature tetragonal phase to a high-temperature average NaCl phase associated with a 16% change in the volume of a supercell. Figure 8 shows lattice constants as a function of temperature for the MD run on KN_3.

In any event, isotropic disordering of the N_3^- ions should lead to a cubic symmetry in KN_3, RbN_3, and CsN_3. However, the prototypic simple cubic sublattice of the disordered N_3^- ions is intrinsically unstable. Our simulations, in agreement with experiment, show that relatively large Cs^+ cations can inhibit this instability allowing the lattice to expand in the CsCl prototypic symmetry to the point where it can accommodate the N_3^- rotations. For RbN_3 and KN_3 our results indicate that this is no longer true. Rb^+ and K^+, being

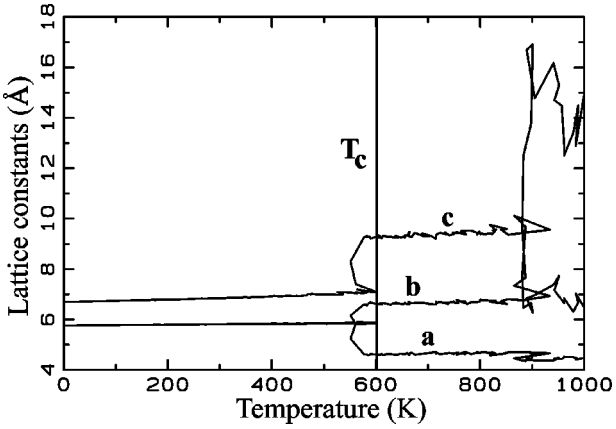

FIG. 8. Lattice constants as a function of temperature for the MD run on KN_3. See Fig. 6 for the description of the structural transformation.

smaller, cannot sufficiently inhibit the intrinsic instability of the N_3^- sublattice which, along with the cation sublattice, transforms to the fcc symmetry as the expansion proceeds to allow for the N_3^- rotations. This creates the average NaCl high-temperature phase of RbN_3 and KN_3. We found that for RbN_3 this transformation is somewhat separated from the onset of the N_3^- disordering whereas in KN_3 disordering and restructuring take place simultaneously. In reality, the very large volume change of 19% and 16% associated with these sc→fcc transitions in RbN_3 and KN_3 will, at some point, induce melting rather than transformation. [These changes should be compared with the ~30% change in the volume/ion pair on going from sc→fcc for fixed nearest-neighbor distance. The discrepancy clearly demonstrates that in the sc (CsCl) phase the lattice constant is strongly influenced by N_3^--N_3^- (second-neighbor) interactions.] The transient, disordered phase found experimentally over 2 K in RbN_3 (Table II) corresponds to the disordered but not yet transformed phase in our MD runs. Similarly, the absence of the high-temperature disordered phase of KN_3 in experiment may be explained by the rapid commencement of the restructuring upon the onset of disordering in this material.

V. CONCLUSION

We have shown that our parameter-free potentials reproduce the room-temperature phases of KN_3, RbN_3, and CsN_3 to a high degree of accuracy. We subsequently used these potentials in MD runs to study the order-disorder transitions in these materials. Our results show that disordering in all three azides is of the form of hindered rotations about all three axes, and that in KN_3 and RbN_3 this disordering is

TABLE II. Calculated and experimental values of T_c and experimental melting points for KN_3, RbN_3, and CsN_3. Experimental values are taken from Ref. 9.

	KN_3	RbN_3	CsN_3
T_c theory (K)	600	620	480
T_c experiment (K)		588	424
Melting experiment (K)	618	590	599

associated with restructuring to a new average NaCl phase. However, in the real KN_3 and RbN_3 systems the large volume changes induce melting rather than structural transformations. In CsN_3 the N_3^- ions disorder in the prototypic average CsCl phase.

ACKNOWLEDGMENTS

This work was supported by the U.S. Army Research Office under Grant Nos. DAAG 55-97-1-0106 and DAAG 55-98-1-0273.

[1] A. Fuith, Phase Transit. **62**, 1 (1997).
[2] H. M. Lu and J. R. Hardy, Phys. Rev. B **42**, 8339 (1990).
[3] R. G. Gordon and Y. S. Kim, J. Phys. Chem. **56**, 3122 (1971).
[4] M. J. Frish, Æ. Frish, and J. Foresman, GAUSSIAN94 (Gaussian, Pittsburgh, PA, 1994).
[5] R. S. Mulliken, J. Phys. Chem. **23**, 1833 (1955).
[6] E. Clementi and C. Roetti, At. Data Nucl. Data Tables **14**, 177 (1974).
[7] U. Mller, Z. Anorg. Allg. Chem. **398**, 159 (1972).
[8] C. S. Choi and E. Prince, J. Phys. Chem. **64**, 4510 (1976).
[9] H. J. Mueller and J. A. Joebstl, Z. Kristallogr. **121**, 385 (1965).
[10] Z. Iqbal and C. W. Christoe, J. Phys. Chem. **62**, 3246 (1975).
[11] F. J. Owens, J. Phys. C **12**, 2255 (1979).
[12] A preliminary account of this work was presented by M. M. Ossowski and J. R. Hardy, at *The Second International Conference on Modeling and Simulations of Microsystems, San Juan, Puerto Rico, 1999* (Computational Publications, Cambridge, MA, 1999).